

PaReNTT: Low-Latency Parallel Residue Number System and NTT-Based Long Polynomial Modular Multiplication for Homomorphic Encryption

Weihang Tan, *Student Member, IEEE*; Sin-Wei Chiu, *Student Member, IEEE*; Antian Wang, *Student Member, IEEE*; Yingjie Lao, *Senior Member, IEEE*; and Keshab K. Parhi, *Fellow, IEEE*

Abstract—High-speed long polynomial multiplication is important for applications in homomorphic encryption (HE) and lattice-based cryptosystems. This paper addresses low-latency hardware architectures for long polynomial modular multiplication using the number-theoretic transform (NTT) and inverse NTT (iNTT). Chinese remainder theorem (CRT) is used to decompose the modulus into multiple smaller moduli. Our proposed architecture, namely PaReNTT, makes four novel contributions. First, parallel NTT and iNTT architectures are proposed to reduce the number of clock cycles to process the polynomials. This can enable real-time processing for HE applications, as the number of clock cycles to process the polynomial is inversely proportional to the level of parallelism. Second, the proposed architecture eliminates the need for permuting the NTT outputs before their product is input to the iNTT. This reduces latency by $n/4$ clock cycles, where n is the length of the polynomial, and reduces buffer requirement by one delay-switch-delay circuit of size n . Third, an approach to select special moduli is presented where the moduli can be expressed in terms of a few signed power-of-two terms. Fourth, novel architectures for pre-processing for computing residual polynomials using the CRT and post-processing for combining the residual polynomials are proposed. These architectures significantly reduce the area consumption of the pre-processing and post-processing steps. The proposed long modular polynomial multiplications are ideal for applications that require low latency and high sample rate as these feed-forward architectures can be pipelined at arbitrary levels. The experimental results show that the proposed architecture reduces the area-block processing product (ABP) by a factor of 43.2 times with respect to LUT and 11.5 times with respect to DSP, when compared without the use of CRT, for a polynomial degree of 4096 and word-length of 192 bits, for a two-parallel architecture.

Index Terms—Polynomial modular multiplication, Parallel NTT/iNTT, Residue Number System, Moduli Selection, Lattice-based Cryptography, Homomorphic Encryption

I. INTRODUCTION

Privacy-preserving protocols and the security of the information are essential for cloud computing. To this end, cloud platforms typically encrypt the data by certain conventional symmetric-key or asymmetric-key cryptosystems to protect

This research was supported in part by the Semiconductor Research Corporation under contract number 2020-HW-2998. Weihang Tan and Sin-Wei Chiu contributed equally to this work.

Weihang Tan, Antian Wang, and Yingjie Lao are with the Holcombe Department of Electrical and Computer Engineering, Clemson University, Clemson, SC 29634, USA. E-mail: {wtan, antianw, ylao}@clemson.edu

Sin-Wei Chiu, and Keshab K. Parhi are with Department of Electrical and Computer Engineering, University of Minnesota, Minneapolis, MN 55455, USA. E-mail: {chiu0091, parhi}@umn.edu

user privacy. However, these methods cannot prevent information leakage during the computation on the cloud since the data must be decrypted before the computation. To further enhance privacy, homomorphic encryption (HE) has emerged as a promising tool that can guarantee the confidentiality of information in an untrusted cloud. Homomorphic encryption is also deployed in privacy-preserving federated learning [1] and neural network inference [2].

Homomorphic multiplication and homomorphic addition are two fundamental operations for the HE schemes. Most of the existing HE schemes are constructed from the ring-learning with errors (R-LWE) problem [3] that adds some noise to the ciphertext to ensure post-quantum security. However, the quadratic noise growth of homomorphic multiplication requires the ciphertext modulus to be very large, which results in inefficient arithmetic operations. One possible solution to address this issue is to decompose the modulus and execute it in parallel. This approach has been used in residue number system (RNS) representation. In the literature, RNS-based implementations have been employed in several software [4], [5] and hardware implementations [6]–[8]. However, RNS relies on the Chinese remainder theorem (CRT), which requires additional pre-processing and post-processing operations. The hardware building blocks for these steps need to be optimized; otherwise, the complexity of the RNS system will negate the advantages of parallelism of the RNS. Meanwhile, modular polynomial multiplication is one of the essential arithmetic operations for the R-LWE problem-based cryptosystems and, indeed, HE schemes. The complexity of the number-theoretic transform (NTT)-based modular polynomial multiplication can be reduced dramatically compared to the schoolbook-based modular polynomial multiplication.

Different modular long polynomial multiplier architectures can be adopted for different applications. For example, a low-area time-multiplexed architecture is well-suited for an edge device. However, the cloud requires very high-speed architectures where multiple coefficients of the polynomial need to be processed in a clock cycle. This inherently requires a parallel architecture where the level of parallelism corresponds to the number of coefficients processed in a clock cycle. While substantial research has been devoted to designing and implementing sequential and time-multiplexed architectures, much less research on parallel NTT-based architectures has been presented. Computing the inverse NTT (iNTT) of the product of NTT of the two polynomials in the can lead to long

latency and extra buffer requirement if its scheduling aspects are not considered as the product needs to be shuffled before the iNTT is computed.

Although parallel NTT-based architectures can achieve low latency and high speed, these require a large silicon area for the arithmetic operations as the word-lengths of the coefficients can be large. To reduce the area, residue arithmetic is used to convert the coefficient into several smaller coefficients that can be implemented using shorter word-lengths. This paper proposes parallel residue arithmetic and NTT-based modular long polynomial multiplication referred to as PaReNTT. The use of different scheduling (folding) of the NTT and iNTT operations eliminates the need for additional buffers. Thus, the latency of the complete operation is reduced. Use of parallel NTT architecture reduces the number of clock cycles needed to process the long polynomial modular multiplication. The proposed parallel NTT and iNTT architectures are completely feed-forward and achieve full hardware utilization. These can be pipelined at any arbitrary level. To the best of our knowledge, the proposed architecture is the first approach for feed-forward and parallel NTT-based implementation that eliminates intermediate shuffling or buffer requirement.

Fig. 1 shows the overview of the proposed PaReNTT architecture, which can be broken down into three steps. The first step, referred to as residual polynomials computations (pre-processing operation), splits the two input polynomials into several polynomials whose coefficients are small. Then, instead of using only one modular polynomial multiplier, several modular polynomial multiplications are executed in parallel in the residual domain. Finally, the post-processing operation performs the inverse mapping for the product polynomials to one polynomial using the CRT. The result is the same as directly performing the modular polynomial multiplication for two input polynomials. In the literature, most CRT and NTT-based modular polynomial multipliers are based on feedback architectures with loops for executing multiple operations in a time-multiplexed manner [6], [7], [9]. In particular, these prior works consider a unified architecture for the NTT and iNTT architecture, which is typically constructed from a memory-based or folded architecture framework. This design strategy can reduce the number of required processing elements (PEs). However, a feedback architecture requires feeding the intermediate results to the storage (memories or registers) and returning back to the input port of the architecture via the loops in multiple cycles. This method does not allow continuous loading of the new inputs, since the input/output unit (I/O) is occupied by the intermediate results. Different from the prior works, our proposed architecture exploits a feed-forward and parallel architecture. Our proposed architecture has no feedback loops/data paths. Therefore, the intermediate results can be executed and passed through to the next stage PE directly. The contributions of this paper are four-fold and are summarized below.

- We propose a novel *parallel* NTT-based polynomial multiplier where the number of clock cycles to process the coefficients of the polynomials is inversely proportional to the level of parallelism. This real-time architecture

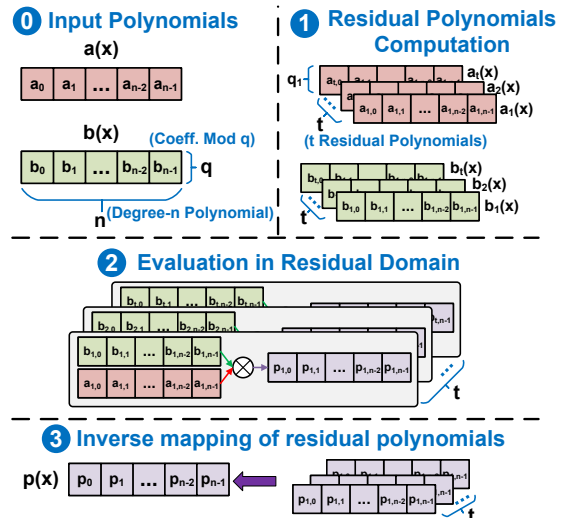


Fig. 1. Overview of the use of residue arithmetic and CRT in the proposed PaReNTT architecture.

requires a linear increase in area with respect to the level of parallelism.

- Our proposed architecture does not require intermediate shuffling operations. Different folding sets for the NTT and iNTT are used such that the product of the two NTTs can be processed immediately in the iNTT. This leads to a significant reduction in latency and complete elimination of intermediate buffer requirement.
- We propose a CRT-based implementation for the modular multiplication, which allows each NTT-based polynomial multiplication to operate over a small prime (co-prime factor). A special format of primes is also considered to reduce the cost of the implementation. Specifically, all the primes are not only NTT-compatible and CRT-friendly but also have low Hamming weights (i.e., these contain only a few signed power-of-two terms).
- Novel optimized architectures for pre-processing and post-processing for residue arithmetic are proposed; these architectures reduce area and power consumption. Finally, the low-cost pre-processing and post-processing blocks for the residue arithmetic are integrated into the parallel NTT-based modular polynomial multiplier to achieve high speed, low latency, and low area designs. In particular, optimizations in the pre-processing step can replace $(t - 1)$ Barrett reduction units with only one Barrett reduction unit. The optimized post-processing step has a lower cost since it bypasses any expensive modular multipliers over a large modulus q .

The rest of this paper is organized as follows: Section II reviews the mathematical background for the RNS and NTT-based polynomial modular multiplication and the corresponding hardware architectures in prior works. Section III presents a parallel architecture for the NTT-based polynomial multiplication that eliminates intermediate storage requirements. Then, Section IV introduces our optimized RNS and CRT-based polynomial multiplier. The performance of our proposed architecture is presented and analyzed in Section V. Finally, Section VI concludes the paper.

II. BACKGROUND

A. Notation

For a polynomial ring $R_{n,q} = \mathbb{Z}_q[x]/(x^n + 1)$, its coefficients have to be modulo q (i.e., these lie in the range $[0, q - 1]$) and the degree of the polynomial is less than n (n is a power-of-two integer). To ensure all the intermediate results will not exceed such a polynomial ring, a modular reduction operation is needed, which is expressed as “mod $(x^n + 1, q)$ ” or $[\circ]_q$. The polynomial of the ring $R_{n,q}$ is denoted as $a(x) = \sum_{j=0}^{n-1} a_j x^j$, where the j -th coefficient inside the polynomial $a(x)$ is represented as a_j .

The addition and multiplication of two polynomials modulo $(x^n + 1, q)$ (i.e., modular polynomial addition and multiplication) are written as $a(x) + b(x)$ and $a(x) \cdot b(x)$, respectively. We also use \odot to denote the point-wise multiplication over $(x^n + 1, q)$ between two polynomials. Parameters $m = \log_2 n$ and $s \in [0, m - 1]$ represent the total number of stages and the current stage in the NTT (iNTT), respectively.

B. Homomorphic encryption and residue number system

HE allows the computations (e.g., multiplication, addition) directly on the ciphertext, without decryption, so that the users can upload their data to any (even untrusted) cloud servers while preserving privacy. The HE schemes can be broadly classified as fully HE (FHE) and somewhat HE (SHE). The FHE schemes allow an arbitrary number of homomorphic evaluations while suffering from high computational complexity [10]. SHE is an alternative solution with better efficiency than the FHE, which only allows performing a limited number of operations without decryption [3], [11], [12].

High-level steps for HE schemes can be summarized in four stages: key generation, encryption, evaluation, and decryption. In particular, the key generation step is used to output three keys: the secret key, public key, and relinearization key, based on the security parameter λ . Then, using the public key, the encryption algorithm encrypts a message into a ciphertext ct . During the evaluation step, a secure evaluation function performs a computation homomorphically for all input ciphertexts and outputs a new ciphertext ct' using the relinearization key. Finally, the result can be obtained using the secret key and ct' in the decryption step.

Key generation, encryption, and decryption steps are generally executed by the client. Meanwhile, the evaluation step is distributed to the cloud server for homomorphic computation. Different homomorphic evaluation functions have different computational costs. The homomorphic addition is relatively simple since it is implemented by modular polynomial additions. However, homomorphic multiplication requires expensive modular polynomial multiplication. Thus the hardware or software accelerations for the modular polynomial multiplier, especially under the HE parameters with large degrees of polynomial and long word-length coefficients, are demanding.

As an example, performing a depth of four homomorphic multiplications with an 80-bit security level requires a 180-bit ciphertext modulus and degree-4096 polynomial in prior works [7]. However, the computation involving the long

word-length coefficients is not trivial, which is also inefficient without high-level transformations. Since the moduli in most widely-used SHE schemes, e.g., BGV [3], BFV [11], CKKS [12], are not restricted to be primes, it is possible to choose each modulus to be a product of several distinct primes by using CRT, where each prime is an NTT-compatible prime with a small word-length.

The CRT algorithm decomposes q to q_1, q_2, \dots, q_t (i.e., $q = \prod_{i=1}^t q_i$, q_i 's are mutually co-prime), and the ring isomorphism $R_q \cong R_{q_1} \times R_{q_2} \times \dots \times R_{q_t}$. After this decomposition, ring operation in each R_{q_i} is performed separately, which thus can be executed in parallel. From the implementation perspective, the larger the parameter t , the smaller each q_i and the simpler arithmetic operation over R_{q_i} .

C. Prior hardware implementations

Several hardware architectures based on CRT-based optimization have been proposed in [6], [7], [9], [13]. The works in [6], [7] introduce an approximate CRT method for the BFV scheme, which involves the lifting and scaling operations to switch between a small ciphertext modulus q and a large ciphertext modulus Q . Later, a multi-level parallel accelerator utilizing the RNS and NTT algorithms is presented in [9]. Nevertheless, these works mainly focus on optimizing the NTT blocks but not on the CRT system's pre-processing and post-processing functional blocks.

III. PARALLEL NTT-BASED POLYNOMIAL MULTIPLIER WITHOUT SHUFFLING OPERATIONS

The long polynomial degree n can be in the range of thousands for the HE schemes, which becomes the bottleneck for the implementations in both software and hardware [14], [15]. Therefore, an efficient NTT-based polynomial multiplication method with a time complexity of $\mathcal{O}(n \log n)$ is used. This method significantly reduces the time complexity compared to the $\mathcal{O}(n^2)$ complexity method of the schoolbook polynomial multiplication along with the modular polynomial reduction.

A. NTT-based polynomial multiplication using negative wrapped convolution

The prior work in [16] presents an efficient algorithm for the NTT-based polynomial multiplication computing $p(x) = a(x) \cdot b(x) \bmod (x^n + 1, q)$, namely negative wrapped convolution, as shown in Algorithm 1. Note that the weighted operations are needed before NTT and after iNTT during the negative wrapped convolution to avoid the expensive zero padding [16].

The core step of this algorithm is the NTT that converts the polynomials $a(x)$ and $b(x)$ to their NTT-domain $\tilde{A}(x)$ and $\tilde{B}(x)$ as in Step 2. The NTT for polynomial $a(x)$ is mathematically expressed as

$$\tilde{A}_k = \sum_{j=0}^{n-1} a_j \psi_{2n}^j \omega_n^{kj} \bmod q, \quad k \in [0, n-1]. \quad (1)$$

Polynomial $b(x)$ is similarly transformed to $\tilde{B}(x)$. Specifically, ω is the primitive n -th root of unity modulo q (i.e., twiddle factor), which satisfies $\omega^n \equiv 1 \bmod q$. ψ_{2n} is the primitive

$2n$ -th root of unity modulo q , and thus $\omega = \psi_{2n}^2 \pmod q$. After using the NTT algorithm, the efficient point-wise multiplication between $\tilde{A}(x)$ and $\tilde{B}(x)$ is performed, which is followed by the iNTT. The iNTT transforms product, \tilde{P} , to the original algebraic domain polynomial $p(x)$, which is defined as

$$p_k = n^{-1} \psi_{2n}^{-k} \sum_{j=0}^{n-1} \tilde{P}_j \omega_n^{-kj} \pmod q, \quad k \in [0, n-1], \quad (2)$$

where n^{-1} is the modular multiplicative inverse of n with respect to modulo q .

During the NTT and iNTT, the weighted operation requires the multiplication of the polynomials by the weights $\psi_{2n}^j \pmod q$ for NTT or $\psi_{2n}^{-j} \pmod q$ for iNTT. Furthermore, an NTT-compatible prime is also utilized, i.e., q must satisfy that $(q-1)$ is divisible by $2n$.

Since the weighted operations in NTT/iNTT require a large number of expensive modular multiplications, the recent works in [17], [18] present a new method to merge the weighted operations into the butterfly operations. In particular, the new NTT in Equation (1) is re-represented as \tilde{A}_k and $\tilde{A}_{k+n/2}$ by using the decimation-in-time (DIT) method:

$$\tilde{A}_k = a_k^\diamond + \psi_{2n} \omega_n^k a_k^\square \pmod q, \quad (3)$$

$$\tilde{A}_{k+n/2} = a_k^\diamond - \psi_{2n} \omega_n^k a_k^\square \pmod q, \quad (4)$$

where $k \in [0, \frac{n}{2} - 1]$ and

$$a_k^\diamond = \sum_{j=0}^{n/2-1} a_{2j} \psi_{2n}^j \omega_n^{kj} \pmod q, \quad (5)$$

$$a_k^\square = \sum_{j=0}^{n/2-1} a_{2j+1} \psi_{2n}^j \omega_n^{kj} \pmod q. \quad (6)$$

Since $\omega = \psi_{2n}^2 \pmod q$, the integers ψ_{2n}^j and ω_n^{kj} can be merged as an integer $\psi_{2^{j+1}n/2^s}$ in the s -th stage; Thus, only one multiplication is required in the butterfly operation, and the architecture is shown in Fig. 2.

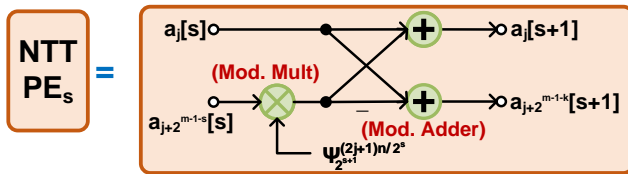


Fig. 2. Architecture for DIT-based butterfly with merging the weighted operation in NTT.

The improved iNTT algorithm merges not only the weighted operation but also the multiplication with constant n^{-1} into the butterfly operations, as presented in [17]. Based on Equation (2) and the decimation-in-frequency (DIF) method, the new iNTT algorithm is expressed as

$$p_{2k} = \frac{n-1}{2} \psi_n^{-k} \sum_{j=0}^{n/2-1} \tilde{P}_j^{even} \omega_n^{-kj} \pmod q, \quad (7)$$

$$p_{2k+1} = \frac{n-1}{2} \psi_n^{-k} \sum_{j=0}^{n/2-1} \tilde{P}_j^{odd} \omega_n^{-kj} \pmod q, \quad (8)$$

where $k \in [0, \frac{n}{2} - 1]$, and

$$\tilde{P}_j^{even} = \frac{\tilde{P}_j + \tilde{P}_{j+n/2}}{2} \pmod q \quad (9)$$

$$\tilde{P}_j^{odd} = \frac{\tilde{P}_j - \tilde{P}_{j+n/2}}{2} \omega_n^{-j} \psi_{2n}^{-1} \pmod q. \quad (10)$$

Similarly, the integers ω_n^{-j} and ψ_{2n}^{-1} are combined as an integer $\psi_{2^{j+1}n/2^s}$ in the s -th stage. Different from the NTT butterfly architecture, the modular addition and modular subtraction intermediate results in the iNTT butterfly need to be divided by two. Fig. 3 shows a hardware-friendly architecture, which only involves one left shift operation, one modular addition with constant $\frac{q+1}{2}$, and one multiplexer (MUX) for one modular division by two [19].

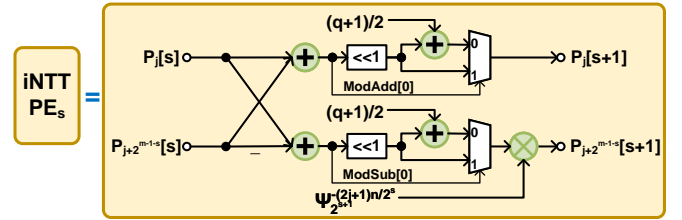


Fig. 3. Architecture for DIF-based butterfly with merging the weighted operation in iNTT.

Algorithm 1 Negative Wrapped Convolution [16]

Input: $a(x), b(x) \in R_{n,q}$

Output: $p(x) = a(x) \cdot b(x) \pmod{(x^n + 1, q)}$

- 1: $\tilde{a}(x) = \sum_{j=0}^{n-1} a_j \psi_{2n}^j x^j \pmod q$
- 2: $\tilde{b}(x) = \sum_{j=0}^{n-1} b_j \psi_{2n}^j x^j \pmod q$
- 3: $\tilde{A}(x) : A_k = \sum_{j=0}^{n-1} \tilde{a}_j \omega_n^{kj} \pmod q, k \in [0, n-1]$
- 4: $\tilde{B}(x) : B_k = \sum_{j=0}^{n-1} \tilde{b}_j \omega_n^{kj} \pmod q, k \in [0, n-1]$
- 5: $\tilde{P}(x) = \tilde{A}(x) \odot \tilde{B}(x) = \sum_{k=0}^{n-1} \tilde{A}_k \tilde{B}_k x^k$
- 6: $\tilde{p}(x) = n^{-1} \sum_{j=0}^{n-1} \tilde{P}_j \omega_n^{-kj} \pmod q, k \in [0, n-1]$
- 7: $p(x) = \sum_{j=0}^{n-1} \tilde{p}_j \psi_{2n}^{-j} x^j$

B. Two-parallel architecture

We propose a novel real-time, feed-forward, and parallel NTT-based polynomial multiplication architecture design that does not require intermediate shuffling, as shown in Fig. 4.

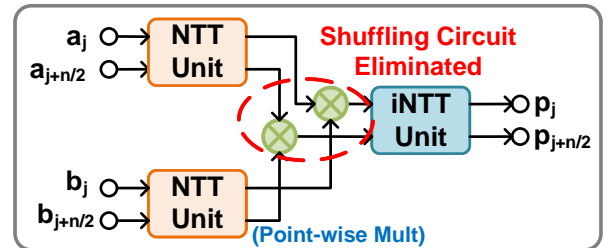


Fig. 4. Architecture for the modular polynomial multiplier using two-parallel NTT/iNTT units. In particular, the NTT/iNTT units in Fig. 4 are based on a two-parallel architecture; these are derived using appropriate folding sets and the folding transformation [20], [21]. Fig. 5 and Fig. 6 show the data-flow graphs for 16-point forward

NTT of $a(x)$ and iNTT for $P(x)$, respectively, where each circle represents one butterfly operation.

After applying the folding transformation, the operations in the same color are fed into the same PE and then executed in a time-multiplexed manner. The order in which the butterfly operations are executed in the same PE is referred to as the folding order. Also, the corresponding clock cycle for each butterfly operation is highlighted in blue in Fig. 5 and Fig. 6. In this 16-point example, the folding set (i.e., the ordered set of operations executed in each PE) of the forward NTT is expressed as:

$$\begin{aligned} A &= \{A_0, A_1, A_2, A_3, A_4, A_5, A_6, A_7\} \\ B &= \{B_4, B_5, B_6, B_7, B_0, B_1, B_2, B_3\} \\ C &= \{C_2, C_3, C_4, C_5, C_6, C_7, C_0, C_1\} \\ D &= \{D_1, D_2, D_3, D_4, D_5, D_6, D_7, D_0\}. \end{aligned} \quad (11)$$

An additional shuffling circuit is typically used for reordering

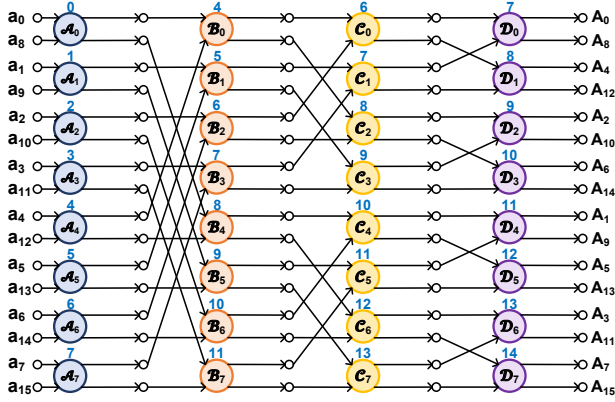


Fig. 5. Data-flow graph of the 16-point forward NTT.

output data before computing iNTT. However, such a shuffling circuit requires a large number of clock cycles and registers.

In the proposed novel architecture, the two-parallel products are fed into a two-parallel iNTT architecture such that no intermediate buffer is needed. Thus, the outputs of the product are executed immediately by the iNTT. This is possible as we can select different folding sets for the NTT and iNTT. It

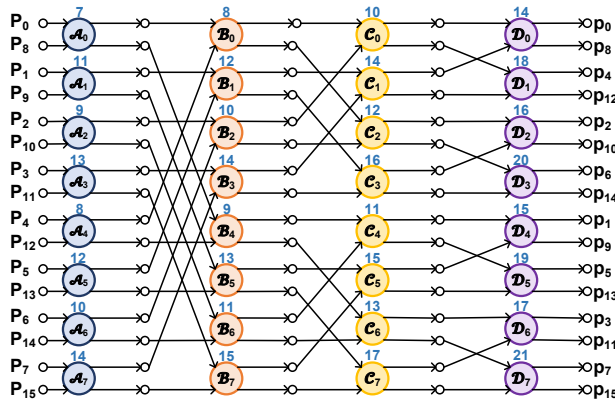


Fig. 6. Data-flow graph of the 16-point iNTT.

may be noted that reconfigurable memory-based NTT-based polynomial multipliers have been published in [9], [17], [22]–[25]. However, the intermediate results and the twiddle factors

in the NTT/iNTT algorithm have data dependencies. As a result, the memory-based architectures easily have control/data hazards and cause bubbles in the pipeline, which will waste extra clock cycles [6]. In order to avoid intermediate buffer or data format conversion from NTT to iNTT, the output samples from the last PE in the NTT unit should be fed into the first PE in the iNTT unit at the same clock cycle. This is achieved using the following folding set for the iNTT:

$$\begin{aligned} A &= \{A_4, A_2, A_6, A_1, A_5, A_3, A_7, A_0\} \\ B &= \{B_0, B_4, B_2, B_6, B_1, B_5, B_3, B_7\} \\ C &= \{C_3, C_7, C_0, C_4, C_2, C_6, C_1, C_5\} \\ D &= \{D_2, D_6, D_1, D_5, D_3, D_7, D_0, D_4\}. \end{aligned} \quad (12)$$

The NTT and iNTT designs are inspired by the design of parallel FFT architectures based on folding sets [26], [27]. Parallel NTT architectures based on folding sets was presented in our earlier work [28]. The NTT architecture in Fig. 7 is derived using the folding sets shown in Equation (11). Specifically, this architecture has four PEs and three delay-switch-delays (DSDs), where the structures for PE and DSD are illustrated in Fig. 2 and Fig. 8. Besides, the DSD block utilizes two MUXs and two register sets, such that it can store the specific data in the data-path and then either switch or pass the data to the PE. Note that the number of registers inside each register set is varied in different stages. In the s -th stage, each register set has 2^{m-s-2} registers in the DSD block for the NTT architecture.

Furthermore, the architecture for iNTT is shown in Fig. 9, and its components are described in Fig. 3 and Fig. 8. One of the main differences between NTT and iNTT architectures is the number of registers located inside each DSD block since they are determined by the folding set as in Equation (12). Specifically, 2^s registers are required for each register set in the s -th stage for the iNTT architecture. Even though the operations of NTT and iNTT are very similar, we consider two separate architectures instead of considering a unified and reconfigurable architecture. The rationale is as follows. Since modular multiplications are heavily used in homomorphic multiplication, using two different architectures for NTT and iNTT allows a continuous flow of the input polynomials and thus can highly accelerate the HE multiplication.

The 16-point architectures in Fig. 7 and Fig. 9 can also be easily generalized to any power-of-two length n by having m PEs and $(m-1)$ DSDs blocks. Furthermore, the general case NTT and iNTT folding sets are defined as follows. We denote the PE in s -th stage as PE_s , and the NTT folding set for the butterfly operations performed inside this PE are illustrated in Table I. The entries in the Table describe the node index of the node of that stage in the data-flow graph. The folding order describes the clock partition at which the node is executed. For example, a folding order s implies that the node is executed at clock cycle $(n/2)l + s$ where l is an integer. The cardinality of the folding set is $n/2$ as there are $n/2$ operations (nodes) in an NTT stage. Thus the scheduling period is $n/2$.

The folding set for iNTT can also be generalized as in Table II, where the symbol $\langle \circ \rangle$ means the bit-reverse representation

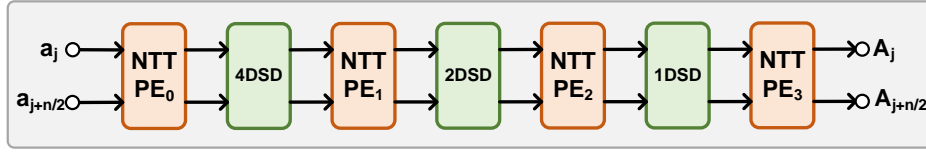


Fig. 7. Architecture of the 16-point forward NTT unit.

TABLE I
GENERALIZED FOLDING ORDER FOR NTT

Folding Order	0	1	...	l	...	$\frac{n}{2} - 1$
PE_0	0	1	...	l	...	$\frac{n}{2} - 1$
PE_1	2^{m-2}	$2^{m-2} + 1$...	$2^{m-2} + l \pmod{\frac{n}{2}}$...	$2^{m-2} - 1$
			...			
PE_s	2^{m-s-1}	$2^{m-s-1} + 1$...	$2^{m-s-1} + l \pmod{\frac{n}{2}}$...	$2^{m-s-1} - 1 \pmod{\frac{n}{2}}$
			...			
PE_{m-1}	1	2	...	$l + 1$...	0

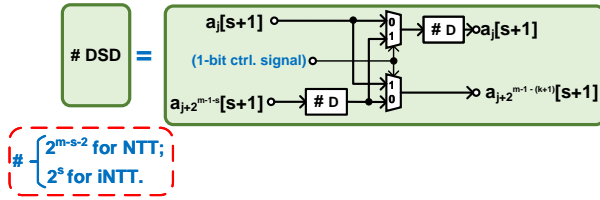


Fig. 8. Architecture for DSD unit.

for the folding set with respect to a $(m-1)$ -bit integer (e.g., $\langle 1 \rangle = \langle 001_b \rangle = 100_b = 4$ when $m = 4$). Specifically, if a node i in the NTT has folding order i , the folding order of the corresponding node in iNTT is $\langle i \rangle - 1$ modulo $(n/2)$. While the bit-reversed scheduling has been known to eliminate latency and buffer requirements at the data-flow graph level, the observation that the same property holds in a parallel NTT-iNTT cascade is non-intuitive and new.

Note that if the iNTT was designed using the same folding set in Equation (11), the product would need to be input to a DSD of size 4 ($n/4$ in general). This would introduce an additional latency of 4 ($n/4$ in general) clock cycles. The use of different folding sets for NTT and iNTT eliminates any additional DSD circuit and its associated latency.

IV. MODULI SELECTION AND ARCHITECTURES FOR PRE-PROCESSING AND POST-PROCESSING FOR CRT

The CRT and NTT-based modular polynomial multiplication can be divided into three stages: pre-processing, NTT-based polynomial multiplication over R_{n,q_i} , and post-processing, with high-level architecture shown in Fig. 10.

A. Special NTT-compatible and CRT-friendly primes selection

As opposed to the prior works that randomly select the co-primes, this paper studies and utilizes the property of the special co-primes to reduce the computational cost and the silicon area. The main idea of this optimization is to trade the flexibility of the co-primes selection for the timing/area performance of the architectures.

In the proposed architecture, each q_i not only needs to be an NTT-compatible prime but also has a short word-length, which is defined as

$$q_i = 2^v - \beta_i, \quad \beta_i = 2^{v_{1i}} \pm 2^{v_{2i}} \pm 2^{v_{3i}} \pm \dots - 1, \quad (13)$$

where v is the word-length of q_i , $\lceil \frac{v-1}{t-1} \rceil > v_{1i} > v_{2i}$, which can ensure q_i to be also CRT-friendly for our later optimization. A CRT-friendly modulus leads to an optimized hardware architecture with respect to the overall timing and area performance for the pre-processing and post-processing steps. Our exhaustive approach generates q_i that are similar to the Solinas prime, and contain a few signed power-of-two terms [29], [30].

The integer multipliers have a larger area consumption and longer delay than the integer adders for the hardware implementation. Besides, the area and delay are proportional to the word-length. Therefore, one possible direction to optimize the modular multiplier, pre-processing stage, and post-processing stage architectures is to reduce the number of integer multipliers, especially the long integer multipliers. In the proposed approach, all the integer multipliers are eliminated when multiplying by q_i , which significantly reduces the computation cost.

B. Residual polynomials computation unit

The pre-processing stage maps the input polynomials to their residual polynomials by applying the CRT algorithm. For the polynomial $a(x)$, its residual polynomials are

$$a_i(x) = [a(x)]_{q_i} = \sum_{j=0}^{n-1} (a_{i,j} \pmod{q_i}) x^j, \quad i \in [1, t]. \quad (14)$$

The same method is applied to the polynomial $b(x)$ to obtain its residual polynomials.

However, this process is not trivial since the word-length of q is much larger than that of q_i . One of the key steps in the pre-processing stage is modular reduction. While Barrett reduction is widely used in modular reduction algorithms for the HE schemes [31], it cannot be directly used in this process since the input for the *efficient* Barrett reduction algorithm has to be

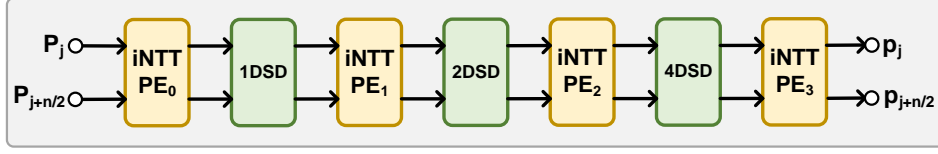


Fig. 9. Architecture of the 16-point iNTT unit.

TABLE II
GENERALIZED FOLDING ORDER FOR INTT

Folding Order	0	1	...	l	...	$\frac{n}{2} - 1$
PE_0	$\langle 1 \rangle$	$\langle 2 \rangle$...	$\langle l + 1 \rangle$...	$\langle 0 \rangle$
PE_1	$\langle 0 \rangle$	$\langle 1 \rangle$...	$\langle l \rangle$...	$\langle 2^{m-1} - 1 \rangle$
			...			
PE_s	$\langle 2 - 2^s \bmod \frac{n}{2} \rangle$	$\langle 2 - 2^s + 1 \bmod \frac{n}{2} \rangle$...	$\langle 2 - 2^s + l \bmod \frac{n}{2} \rangle$...	$\langle 2 - 2^s - 1 \bmod \frac{n}{2} \rangle$
			...			
PE_{m-1}	$\langle 2 \rangle$	$\langle 3 \rangle$...	$\langle l + 2 \bmod \frac{n}{2} \rangle$...	$\langle 1 \rangle$

smaller than q_i^2 when q_i is the modulus. Note that, the original Barrett reduction in [31] utilizes a *while*-loop at the end of the algorithm so there is no restriction for the input word-length. However, it is inefficient for hardware implementation. A more popular hardware implementation method uses an efficient Barrett reduction that replaces the *while*-loop by a simple *if-else* statement and restricts the input word-length.

To utilize the efficient Barrett reduction algorithm for the residual polynomial computation, further transformations in the pre-processing stage are needed. Algorithm 2 presents

Algorithm 2 Efficient residual coefficient computation

Input: $a_j \in [0, q - 1]$, q_i , and $B = 2^v$ ($v = \lceil \log_2(q_i) \rceil$)

Output: $a_{i,j} = a_j \bmod q_i$, $a_{i,j} \in R_{q_i}$

- 1: $a_j = z_0 + z_1 \cdot B + z_2 \cdot B^2 + \dots + z_{t-1} \cdot B^{t-1}$ (Step 1)
- 2: **for** $k = 1$ **to** $t - 1$ **do**
- 3: $r_k = z_k \times \beta_i^k$ // $\beta_i = B \bmod q_i$ (Step 2)
- 4: $a_{i,j} = z_0 + r_1 + \dots + r_{t-1} \bmod q_i$ (Step 3)

Besides, different from the prior work [6] where the Barrett reductions are required to reduce each r_k modulo q_i in Step 2, our design reduces $(t - 1)$ Barrett reduction units to only one required in Step 3. The rationale behind this is as follows. The product r_k in the prior work is a large integer that approximately equals q_i^2 , as β_i^k is any constant modulo q_i . In contrast, since the special q_i 's are used in the proposed design, all the β_i^k are small integers, guaranteeing that all the products, r_k , are sufficiently small.

Since q_i only contains only a few signed power-of-two terms, no integer multiplication is required in Step 2. For example, for a special prime $q_i = 2^v - 2^{v_{1i}} - 2^{v_{2i}} + 1$, β_i in Step 2 can be expressed as

$$\beta_i = [2^v]_{q_i} \equiv 2^{v_{1i}} + 2^{v_{2i}} - 1. \quad (15)$$

Note that more signed-power-two terms can be added to accommodate the desired number of moduli at the cost of an additional adder/subtractor per term.

We use a flow chart for $t = 3$ as an example (illustrated in Fig. 11) to show the overall computation based on this efficient algorithm. It can be seen that the modular multiplication in $z_k \times \beta_i^k$ in [6] (Fig. 12(a)) can be replaced by the shift and add operations, which can reduce the hardware cost. When k becomes larger, a deeper shift and add unit (SAU) is required, as shown in Fig. 11 and Fig. 12(b). However, since a multiplier is typically quadratically more expensive than an adder with respect to word-length, using such a shift and add operation is still much more efficient than using a multiplier to obtain its result r_k . In our CRT-friendly q_i , v_{1i} is at most equal to $(\lceil \frac{v-1}{t-1} \rceil - 1)$ -bits to ensure r_k is smaller than q_i^2 , as shown

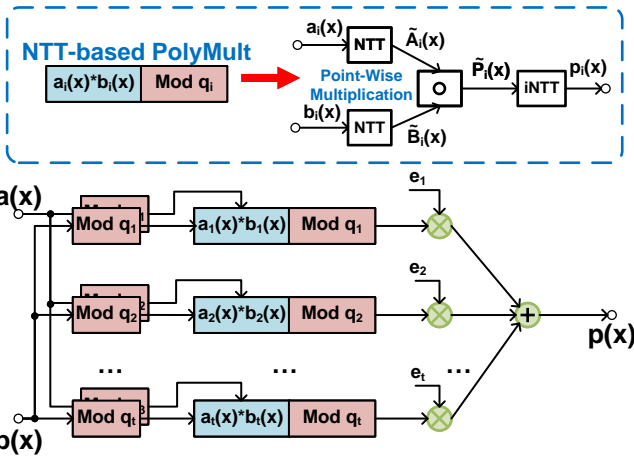
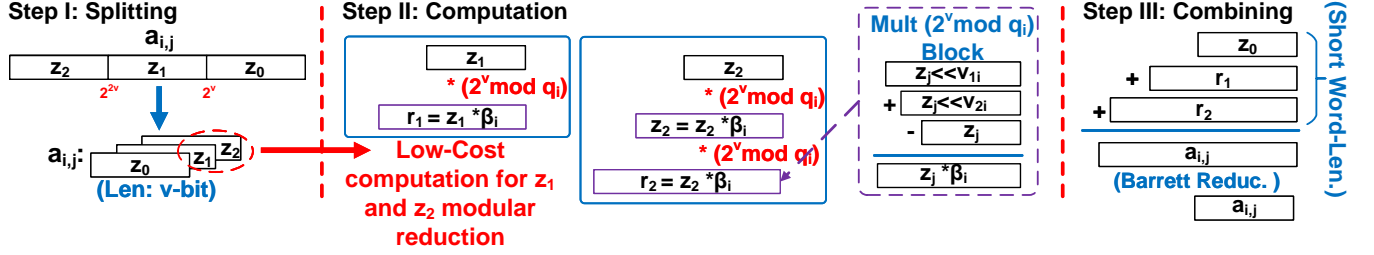
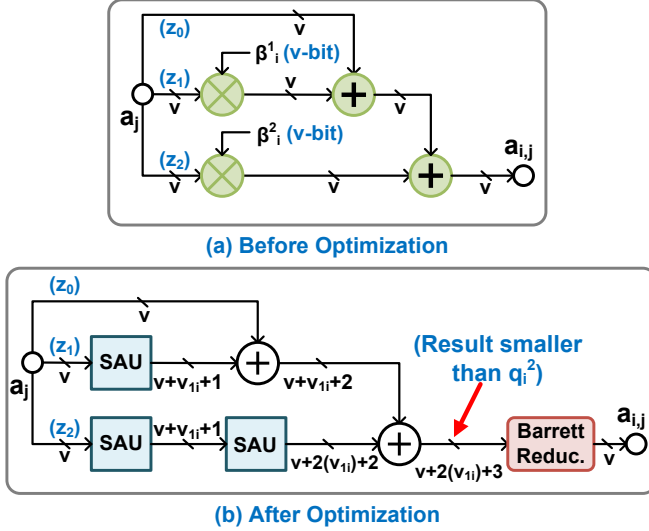


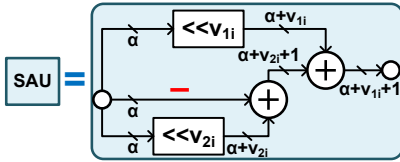
Fig. 10. High-level block diagram of CRT and NTT-based modular polynomial multiplication.

a novel and hardware-friendly optimization to implement Equation (14). For a large integer a_j , the first step is to split it into several segments where each segment has v bits (v is the word-length of q_i). We define the base $B = 2^v$. Thus, each segment in $a_{i,j}$ can be represented as $z_k \cdot B^k$, $k \in [0, t - 1]$. The second step performs the modular reduction for each term, which is the main focus of our hardware optimization.

Since we consider special q_i 's, Step 2 in Algorithm 2 no longer requires $v \times v$ -bit integer multiplication with β_i^k to obtain each r_k . Thus, our proposed method eliminates the expensive modular multiplications.

Fig. 11. Flow chart for the residual coefficient computation unit when $t = 3$.Fig. 12. Top-level architecture of residual coefficient computation unit when $t = 3$.

in Fig. 12(b). Thus, since the operating segments r_k are still represented in short word-lengths, combining all the r_k and z_0 to obtain $a_{i,j}$ only requires adders and a Barrett reduction unit.

Fig. 13. SAU unit of residual coefficient computation unit when $t = 3$ whose input word-length is α .

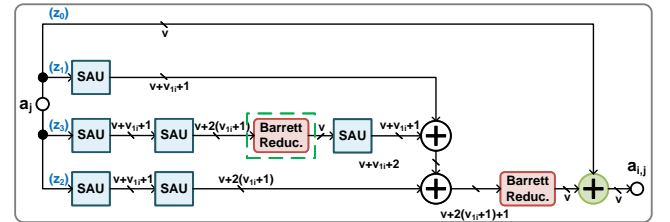
C. Increasing the number of primes when needed

Table III shows the number of special NTT-compatible and CRT-friendly primes that can be found by exhaustive search when 3, 4, and 5 signed power-of-two-terms are considered when $n = 1024$, and each co-prime factor is 48-bit. It can be noticed that the number of generated co-prime factors is not enough for constructing a modulus with four co-prime factors when $n = 1024$ or $n = 4096$ in Table III. However, this bottleneck can be overcome by either using more signed power-of-two terms to construct the co-prime factors or using an additional Barrett reduction. Using the latter method, the co-primes factors for $t = 3$ can also be used in the $t = 4$ case. This approach is used in the experimental evaluation in the paper.

Fig. 14 shows an example for the residual polynomials computation unit with more flexible co-prime factors selection when $t = 4$, $\log_2(q_i) = 48$, and $n = 1024$. Utilizing an additional Barrett reduction unit (inside the green box) can reduce the word-length of the intermediate results, so the co-prime factors for $(t - 1)$ in Table III can be employed. Note that the overhead of this alternative solution is only one Barrett reduction unit and one modular adder, compared to the architecture in Fig. 12(b) when it is in the same parameter setting. Nevertheless, this alternative solution still requires fewer hardware resources than the conventional design in Fig. 12(a) since the number of Barrett reduction units is lower and no integer multiplier is required.

TABLE III
THE NUMBER OF SPECIAL NTT-COMPATIBLE AND CRT-FRIENDLY PRIMES UNDER DIFFERENT SETTINGS WHEN $v = 48$

Parameter Setting	3 terms	4 terms	5 terms
$t = 2, n = 1024, 1 \text{ BR}$	3	98	1501
$t = 3, n = 1024, 1 \text{ BR}$	2	10	34
$t = 4, n = 1024, 1 \text{ BR}$	0	0	0
$t = 4, n = 1024, 2 \text{ BR}$	2	10	34
$t = 2, n = 4096, 1 \text{ BR}$	3	87	1235
$t = 3, n = 4096, 1 \text{ BR}$	2	8	20
$t = 4, n = 4096, 1 \text{ BR}$	0	0	0
$t = 4, n = 4096, 2 \text{ BR}$	2	8	20

Fig. 14. Residual coefficient computation unit with additional Barrett reduction unit when $t = 4$.

D. Evaluation in residual domain

After using CRT representation, the function $f(a_i(x), b_i(x))$ over R_{n,q_i} can be computed independently. As a result, the overall t operations can be executed in parallel. In our case, the function computes the residual products $p_i(x)$ for $i \in [1, t]$, by utilizing NTT-based polynomial multiplication over R_{n,q_i} . The architecture to compute $p_i(x) = a_i(x) \cdot b_i(x) \pmod{(x^n + 1, q_i)}$ is based on our novel NTT-based polynomial multiplier in Fig. 4. Thus, our proposed architecture achieves high throughput and low latency by increasing the parallelism from the CRT representation.

E. Inverse mapping of residual coefficients of polynomials

The results obtained by the evaluation in the residual domain need to be converted back to over the ring $R_{n,q}$, which is the same as $f(a(x), b(x))$ over $R_{n,q}$ (i.e., result computed without using CRT representation).

This post-processing stage is based on the inverse CRT algorithm, which is

$$\begin{aligned} p(x) &= \sum_{i=1}^t p_i(x) \cdot e_i \bmod q \\ &= \sum_{i=1}^t \sum_{j=0}^{n-1} p_{i,j} \cdot e_i \cdot x^j \bmod q, \end{aligned} \quad (16)$$

where each $e_i = q_i^* \cdot \tilde{q}_i$ is a constant, $q_i^* = (\frac{q}{q_i}) \in \mathbb{Z}$, and $\tilde{q}_i = [(\frac{q}{q_i})^{-1}]_{q_i} \in \mathbb{Z}_{q_i}$.

However, direct multiplication by the constant e_i involves a long integer multiplication and expensive modular reduction over q (tv), which will result in an inefficient implementation and a long critical path. Meanwhile, the properties of the special co-primes can lower the cost of modular operations over q_i in the post-processing stage. Therefore, we leverage the technique in [32] to further express Equation (16) as:

$$\begin{aligned} p(x) &= \sum_{i=1}^t [p_i(x) \cdot \tilde{q}_i]_{q_i} \cdot q_i^* \bmod q \\ &= \sum_{i=1}^t \sum_{j=0}^{n-1} [p_{i,j} \cdot \tilde{q}_i]_{q_i} \cdot q_i^* \cdot x^j \bmod q. \end{aligned} \quad (17)$$

Note that the computation in $0 \leq [p_{i,j} \cdot \tilde{q}_i]_{q_i} < q_i$ can be performed efficiently since the modular reduction over q_i has a lower cost than the modular reduction q . As q_i^* is a $(t-1)v$ -bit pre-computed constant, no division is required in the post-processing stage. Besides, the range of the coefficients from $[p_i(x) \cdot \tilde{q}_i]_{q_i} \cdot q_i^*$ is in $[0, q-1]$ so that no modular multiplication is required to compute the product.

The optimized architecture of the inverse mapping of residual coefficients of polynomials is shown in Fig. 15(b) (we use $t = 3$ as an example). In this architecture, each long word-length ($3v \times v$ -bit) multiplier for multiplying e_i is split into $v \times v$ -bit multiplier with constant \tilde{q}_i and $v \times 2v$ -bit multiplier with constant q_i^* . Instead of implementing an expensive modular reduction over a large modulus q block in Fig. 15(a), only two modular adders and three modular reductions over q_i are required to obtain the final result $p(x)$. Specifically, the modular reduction over q_i can reuse the same Barrett reduction block from the pre-processing stage, which is also efficient based on the special co-prime.

Overall, the proposed novel architecture can significantly reduce the area and power consumption.

V. EXPERIMENTAL RESULTS

To evaluate the performance of our proposed design, we first introduce the experimental result of our proposed NTT-based polynomial multiplier, which is based on Section III without the CRT representation as the baseline design for the comparison. Then, the performance of PaReNTT architecture in Section IV (based on the CRT and NTT-based

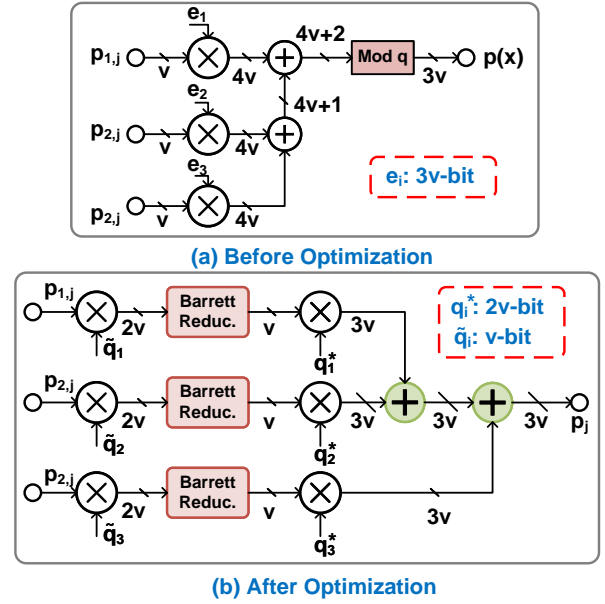


Fig. 15. Inverse mapping architecture when $t = 3$. This circuit illustrates the post-processing step for the inverse CRT.

polynomial multiplier) is presented. The proposed designs are implemented using SystemVerilog and then mapped to Xilinx Virtex Ultrascale FPGA board (XC7VU440-1FLGA2892C, 20nm FinFET node).

We consider three different word-lengths for q (96-bit, 144-bit, and 192-bit) with the same degree of polynomial $n = 1024$ and $n = 4096$ to investigate the designs under different levels of CRT-based parallelism. Specifically, all the decomposed co-prime factors are in 48-bit special NTT-compatible and CRT-friendly format, while the designs without the CRT representation directly utilize the 96-bit, 144-bit, and 192-bit NTT-compatible primes. Note that our design can be easily extended to a longer word-length modulus by either having more co-primes or increasing the word length of each co-prime. Furthermore, each degree-1024 NTT-based polynomial multiplier has 30 PEs and 27 DSD units since $m = \log_2(1024) = 10$. A degree-4096 NTT-based polynomial multiplier applies 36 PEs and 33 DSD units since $m = \log_2(4096) = 12$. Note that a higher degree of the polynomial can be applied, which only requires more PEs and DSDs.

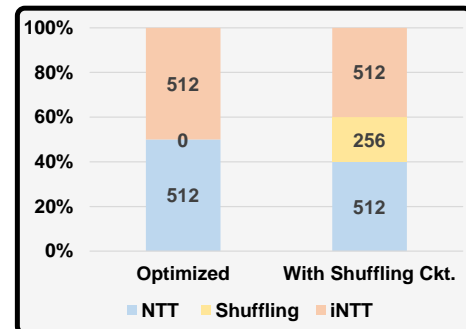


Fig. 16. Comparison of latency of Two-parallel NTT-based polynomial multiplication with and without shuffling operations when $n = 1024$.

A. Evaluation Metrics and Performance of Parallel NTT-based polynomial multiplier for base Modulus

We first describe the evaluation metrics used in this paper. We then evaluate the performance of our NTT-based polynomial multiplier that does not require any shuffling operations.

To analyze the timing performances of the implementations, we define two timing performance metrics, *block processing period* (BPP) and latency. BPP is defined as the time required to process n coefficient inputs or the time required to generate n coefficient outputs. For a degree- n NTT-based two-parallel polynomial multiplier, the expression for BPP is

$$T_{BPP} = n/2, \quad (18)$$

where the throughput is two samples per clock cycle. In addition, the latency for one modular polynomial multiplication is

$$T_{Lat} = (n - 2) + T_{pipe}, \quad (19)$$

where T_{pipe} represents the additional pipelining stages added to the data-path in order to reduce the critical path. Furthermore, the total clock cycles consumed by L modular polynomial multiplications are

$$T_{total} = (T_{BPP} + T_{Lat} - 1) \cdot L. \quad (20)$$

For $n = 1024$, the BPP is 512 clock cycles, and the latency is 1,126 clock cycles (including extra clock cycles required for pipelining). The latency is significantly reduced, compared to the NTT-based polynomial multipliers that use a shuffling circuit in the prior works. The comparison of our optimized and conventional methods (without considering the pipelining) is shown in Fig. 16. Specifically, the conventional method with the shuffling circuit needs additional 256 ($n/4$ in general) clock cycles for the re-ordering, leading to an increase in latency by around 20.0% for a two-parallel design and $n = 1024$.

B. Evaluation on PaReNTT polynomial multiplier

This section considers the implementation of the two-parallel residue arithmetic-based NTT architecture for $n = 1024$ and $n = 4096$. The performances of the two-parallel architecture without and with residue arithmetic (i.e., PaReNTT architecture design) are compared.

For the CRT case, the co-prime factors are 48 bits long (i.e., $v = \log_2(q_i) = 48$), where each co-prime factor has four signed power-of-two terms. Also, the number of co-prime factors, t , increases from 1 to 4.

Tables IV and V, respectively, describe the area and speed (latency) comparisons for a 2-parallel architecture with and without CRT when $n = 1024$. Four word-lengths are considered: 48, 96, 144, and 192 bits. Similarly, the experimental result and comparison when $n = 4096$ are presented for the same word-lengths in Tables VI and VII.

When the word-length increases without using residue arithmetic, the clock frequencies for the FPGA implementation are reduced as shown in Tables V and VII. For example, increasing the word-length from 48-bit to 96-bit results in a 27.1% and 35.6% longer critical path for $n = 1024$ and

$n = 4096$, respectively. Thus, for high-speed applications, the long word-length modulus architecture without the use of residue arithmetic is inefficient.

We now compare the timing performance of the designs with and without residue arithmetic based on the experimental results in Table V for $n = 1024$ and Table VII for $n = 4096$. Note that the implementations with and without the CRT representation have the same stage of pipelining for a fair comparison of the timing performance. When $n = 1024$, the latency of PaReNTT architectures with two, three, and four co-prime factors are reduced by 24.0%, 67.0%, and 88.6% compared to without residue arithmetic implementation. Similarly for $n = 4096$, the latency in the PaReNTT architectures are reduced by 28.5%, 71.0%, and 90.4% for q equal to 96-bit, 144-bit, and 192-bit, respectively. The trends of the delay variation with respect to different word-lengths for PaReNTT architecture design are illustrated in Fig. 17 for $n = 1024$. When the word-length of moduli becomes larger, the logic delay of the CRT-representation architectures remains almost the same as the 48-bit NTT-based polynomial multiplier, while the routing delays increase slightly. Thus, the clock frequencies in CRT-based architectures are similar. However, the delay for the architectures without CRT increases proportionally with respect to the word-length of q .

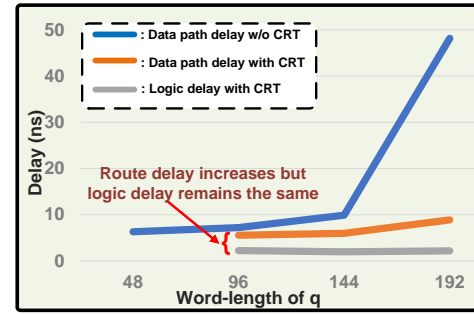


Fig. 17. Delay variation in different word-lengths q when $n = 1024$.

We also examine the area performance of PaReNTT architectures and the implementations without residue arithmetic. The results are presented in Tables IV and VI for $n = 1024$ and $n = 4096$, respectively. Table IV shows the residue arithmetic-based architectures for $n = 1024$ require 26.8%, 48.8%, and 76.9% fewer LUTs when q is a 96-bit, 144-bit, and 192-bit moduli, compared to the implementations without residue arithmetic. For $n = 4096$, residue arithmetic-based architectures require 22.4%, 41.5%, and 75.2% less LUTs for 96-bit, 144-bit, and 192-bit moduli, respectively. Furthermore, the residue arithmetic-based architectures require 46.9%, 53.3%, and 20.8% fewer DSPs for 96-bit, 144-bit, and 192-bit moduli for $n = 1024$, compared to the implementations without residue arithmetic. Similarly, the DSP utilization in the residue arithmetic-based architectures is reduced by 47.4%, 54.1%, and 6.8% for 96-bit, 144-bit, and 192-bit moduli, respectively for $n = 4096$.

We now compare the area-BPP product (ABP) for the PaReNTT architectures and the implementations without residue arithmetic to evaluate the timing and area performance to-

TABLE IV
AREA CONSUMPTION AND FREQUENCY FOR MODULAR POLYNOMIAL MULTIPLIERS WHEN $n = 1024$

$\lceil \log_2 q \rceil$	t	CRT	Freq.[MHz]	LUTs	DSPs	FFs
48	1	No	207	59,426 (2.4%) ^a	288 (10.0%)	15,419 (0.3%)
96	1	No	151	194,016 (7.7%)	1,152 (40.0%)	39,587 (0.8%)
96	2	Yes	199	142,014 (5.6%)	612 (21.3%)	35,655 (0.7%)
144	1	No	54	431,623 (17.0%)	2,080 (72.2%)	62,240 (1.2%)
144	3	Yes	168	221,183 (8.7%)	972 (33.8%)	60,228 (1.2%)
192	1	No	13	1,402,022 (55.4%)	1,696 (58.9%)	145,955 (2.9%)
192	4	Yes	113	323,209 (12.8%)	1,344 (46.7%)	87,150 (1.7%)

^a: # of used resources (% utilization) on FPGA board.

TABLE V
TIMING PERFORMANCE FOR MODULAR POLYNOMIAL MULTIPLIERS WHEN $n = 1024$

$\lceil \log_2 q \rceil$	t	CRT	BPP ^b		Latency ^c		ABP (LUT) ^d	ABP (DSP) ^e
			# Cycles	Period [μ s]	# Cycles	Period [μ s]		
48	1	No	512	2.5	1,126	5.4	0.1M	0.7K
96	1	No	512	3.4	1,126	7.5	0.7M	3.9K
96	2	Yes	512	2.6	1,142	5.7	0.4M	1.6K
144	1	No	512	9.5	1,126	20.9	4.1M	19.7K
144	3	Yes	512	3.0	1,152	6.9	0.7M	3.0K
192	1	No	512	40.7	1,126	89.5	57.0M	69.0K
192	4	Yes	512	4.5	1,152	10.2	1.5M	6.1K

^b: Block processing period (BPP) is the period (μ s) for processing n coefficient inputs or for generating n sample outputs after the first sample out.

^c: Latency is the period (μ s) of the first sample in and the first sample out.

^d: ABP (LUT) is calculated from the number of LUTs times BPP (μ s).

^e: ABP (DSP) is calculated from the number of DSPs times BPP (μ s).

gether. The reductions in ABP(LUT) achieved by the PaReNTT architectures with two, three, and four co-prime factors are 42.9%, 82.9%, and 97.4%, respectively for $n = 1024$. When the degree of polynomial increases to 4096, the reductions for ABP (LUT) are 46.5%, 83.4%, and 97.7%, respectively. When further comparing the ABP (DSP) in a similar way for $n = 1024$, the PaReNTT architectures achieve 59.0%, 84.8%, and 91.2% reductions, respectively. For the degree-4096 case, ABP (DSP) savings in the PaReNTT architectures are 46.5%, 83.4%, and 97.6%, respectively.

C. Comparison to a prior work

Direct comparisons with prior works is difficult as systems are implemented using different datapaths and FPGA devices corresponding to different technologies. Nevertheless, we now compare the proposed design (for $n = 4096$ and $\log_2(q) = 192$) with a prior design ($n = 4096$, $\log_2(q) = 180$) in [7]. The clock frequency and area performance of the prior design are included in the last line of Table VI. Although their design has a better area performance than the PaReNTT architecture, our design has a superior timing performance. Reducing the latency and increasing throughput is the primary goal of this work. The prior design considers a customized optimization for the BFV scheme requiring the lifting and

scaling operations so that the clock cycles for modular multiplication in the homomorphic multiplication are approximately doubled compared to the design without the lifting and scaling operations. To use their design for comparison, we reduce the clock cycles and latency consumption for the CRT-based, NTT, and iNTT operations by a factor of 2. The equivalent number of clock cycles equals $196,003 = (87,582 \times 2 + 102,043 + 15,662 + 99,137)/2$, and the latency is 871.1μ s. Note that the approximated timing results are adopted from Table II in [7] by calculating the sum of two NTTs (for polynomial $a(x)$ and $b(x)$, respectively), coefficient-wise multiplication, iNTT, Lift and then divided by two. Since their scaling step has a more complicated operation than the general inverse mapping for the residual polynomials due to the scheme required, the clock cycles in this step are ignored for their approximated timing result. In the $n = 4096$ and $\log_2(q) = 192$ PaReNTT architecture, the clock cycles for the first data in and last data out is $4,244 + 2,047 = 6,291$ (56.7μ s), which shows that the latency of our design is reduced by a factor of 15.4. Besides we also compare the area-timing product (ATP) for these two designs. The comparison shows that the ATP (LUT) (the product of timing result in μ s and the number of LUTs) and ATP (DSP) (the product of timing result in μ s and the number of DSPs) of our design are 50.1% and 46.6% lower, respectively, compared to the design in [7].

TABLE VI
AREA CONSUMPTION AND FREQUENCY FOR MODULAR POLYNOMIAL MULTIPLIERS FOR $n = 4096$

Design	$\lceil \log_2 q \rceil$	t	CRT	Freq.[MHz]	LUTs	DSPs	FFs
Ours	48	1	No	216	100,681 (4.0%)	342 (11.9%)	20,087 (0.4%)
	96	1	No	139	290,003 (11.5%)	1,368 (47.5%)	48,540 (1.0%)
	96	2	Yes	196	224,964 (8.9%)	720 (25.0%)	43,556 (0.9%)
	144	1	No	47	597,815 (23.6%)	2,470 (85.8%)	69,992 (1.4%)
	144	3	Yes	168	349,720 (13.8%)	1,134 (39.4%)	71,778 (1.4%)
	192	1	No	10	1,965,433 (77.6%)	1,752 (60.8%)	174,852 (3.5%)
	192	4	Yes	111	488,112 (19.3%)	1,632 (56.7%)	101,385 (2.0%)
Roy [7] ^f	180	6	Yes	225	64,000	200	25,000

^f: The design is implemented in Zynq UltraScale+ FPGA board.

TABLE VII
TIMING PERFORMANCE FOR MODULAR POLYNOMIAL MULTIPLIERS FOR $n = 4096$

$\lceil \log_2 q \rceil$	t	CRT	BPP		Latency		ABP	ABP
			# Cycles	Period [μ s]	# Cycles	Period [μ s]	(LUT)	(DSP)
48	1	No	2048	9.5	4,218	19.5	1.0M	3.2K
96	1	No	2048	14.7	4,218	30.2	4.3M	20.1K
96	2	Yes	2048	10.4	4,234	21.6	2.3M	7.5K
144	1	No	2048	43.3	4,218	87.2	25.9M	106.8K
144	3	Yes	2048	12.2	4,244	25.3	4.3M	13.8K
192	1	No	2048	197.8	4,218	398.8	388.8M	346.6K
192	4	Yes	2048	18.5	4,244	38.4	9.0M	30.2K

VI. CONCLUSION

This paper has proposed PaReNTT, an efficient CRT and NTT-based long polynomial multiplier. This design leverages the characteristics of the specially selected primes to optimize the pre-processing and post-processing units for the CRT algorithm. In addition, a novel iNTT unit is designed based on bit-reversed scheduling to eliminate an expensive shuffling circuit and significantly reduce latency. Future work will be directed toward evaluating different homomorphic encryption algorithms such as BFV, BGV, and CKKS using the proposed efficient long polynomial multiplier based on hardware-software co-design.

REFERENCES

- [1] F. Wibawa, F. O. Catak, M. Kuzlu, S. Sarp, and U. Cali, "Homomorphic encryption and federated learning based privacy-preserving CNN training: COVID-19 detection use-case," in *Proceedings of the 2022 European Interdisciplinary Cybersecurity Conference*, 2022, pp. 85–90.
- [2] H. Chen, W. Dai, M. Kim, and Y. Song, "Efficient multi-key homomorphic encryption with packed ciphertexts with application to oblivious neural network inference," in *Proceedings of the 2019 ACM SIGSAC Conference on Computer and Communications Security*, 2019, pp. 395–412.
- [3] V. Lyubashevsky, C. Peikert, and O. Regev, "On ideal lattices and learning with errors over rings," in *Annual International Conference on the Theory and Applications of Cryptographic Techniques*. Springer, 2010, pp. 1–23.
- [4] S. Halevi and V. Shoup, "Algorithms in helib," in *Annual Cryptology Conference*. Springer, 2014, pp. 554–571.
- [5] H. Chen, K. Laine, and R. Player, "Simple encrypted arithmetic library-SEAL v2.1," in *International Conference on Financial Cryptography and Data Security*. Springer, 2017, pp. 3–18.
- [6] S. S. Roy, K. Jarvinen, J. Vliegen, F. Vercauteren, and I. Verbauwhede, "HEPcloud: An FPGA-based multicore processor for FV somewhat homomorphic function evaluation," *IEEE Transactions on Computers*, 2018.
- [7] S. S. Roy, F. Turan, K. Jarvinen, F. Vercauteren, and I. Verbauwhede, "FPGA-based high-performance parallel architecture for homomorphic computing on encrypted data," in *2019 IEEE International Symposium on High Performance Computer Architecture (HPCA)*. IEEE, 2019, pp. 387–398.
- [8] M. S. Riazi, K. Laine, B. Pelton, and W. Dai, "HEAX: An architecture for computing on encrypted data," in *Proceedings of the Twenty-Fifth International Conference on Architectural Support for Programming Languages and Operating Systems*, 2020, pp. 1295–1309.
- [9] G. Xin, Y. Zhao, and J. Han, "A multi-layer parallel hardware architecture for homomorphic computation in machine learning," in *2021 IEEE International Symposium on Circuits and Systems (ISCAS)*. IEEE, 2021, pp. 1–5.
- [10] C. Gentry, *A fully homomorphic encryption scheme*. Stanford university, 2009.
- [11] J. Fan and F. Vercauteren, "Somewhat practical fully homomorphic encryption," *IACR Cryptology ePrint Archive*, vol. 2012, p. 144, 2012.
- [12] J. H. Cheon, A. Kim, M. Kim, and Y. Song, "Homomorphic encryption for arithmetic of approximate numbers," in *International Conference on the Theory and Application of Cryptology and Information Security*. Springer, 2017, pp. 409–437.
- [13] F. Turan, S. S. Roy, and I. Verbauwhede, "HEAWS: An accelerator for homomorphic encryption on the amazon aws fpga," *IEEE Transactions on Computers*, vol. 69, no. 8, pp. 1185–1196, 2020.
- [14] A. Aysu, C. Patterson, and P. Schaumont, "Low-cost and area-efficient FPGA implementations of lattice-based cryptography," in *2013 IEEE International Symposium on Hardware-Oriented Security and Trust (HOST)*. IEEE, 2013, pp. 81–86.
- [15] W. Dai and B. Sunar, "cuHE: A homomorphic encryption accelerator library," in *International Conference on Cryptography and Information Security in the Balkans*. Springer, 2015, pp. 169–186.
- [16] V. Lyubashevsky, D. Micciancio, C. Peikert, and A. Rosen, "SWIFFT: A modest proposal for FFT hashing," in *International Workshop on Fast Software Encryption*. Springer, 2008, pp. 54–72.

- [17] N. Zhang, B. Yang, C. Chen, S. Yin, S. Wei, and L. Liu, "Highly efficient architecture of NewHope-NIST on FPGA using low-complexity NTT/INTT," *IACR Transactions on Cryptographic Hardware and Embedded Systems*, pp. 49–72, 2020.
- [18] P. Longa and M. Naehrig, "Speeding up the number theoretic transform for faster ideal lattice-based cryptography," in *International Conference on Cryptology and Network Security*. Springer, 2016, pp. 124–139.
- [19] Y. Zhang, C. Wang, D. E. S. Kundi, A. Khalid, M. O'Neill, and W. Liu, "An efficient and parallel R-LWE cryptoprocessor," *IEEE Transactions on Circuits and Systems II: Express Briefs*, vol. 67, no. 5, pp. 886–890, 2020.
- [20] K. K. Parhi, *VLSI digital signal processing systems: design and implementation*. John Wiley & Sons, 1999.
- [21] K. K. Parhi, C.-Y. Wang, and A. P. Brown, "Synthesis of control circuits in folded pipelined DSP architectures," *IEEE Journal of Solid-State Circuits*, vol. 27, no. 1, pp. 29–43, 1992.
- [22] Y. Xing and S. Li, "A compact hardware implementation of CCA-secure key exchange mechanism crystals-kyber on fpga," *IACR Transactions on Cryptographic Hardware and Embedded Systems*, pp. 328–356, 2021.
- [23] A. C. Mert, S. Kwon, Y. Shin, D. Yoo, Y. Lee, and S. S. Roy, "Medha: Microcoded hardware accelerator for computing on encrypted data," *IACR Transactions on Cryptographic Hardware and Embedded Systems*, pp. 463–500, 2023.
- [24] A. C. Mert, E. Öztürk, and E. Savaş, "FPGA implementation of a run-time configurable NTT-based polynomial multiplication hardware," *Microprocessors and Microsystems*, vol. 78, p. 103219, 2020.
- [25] R. Paludo and L. Sousa, "NTT architecture for a Linux-ready RISC-V fully-homomorphic encryption accelerator," *IEEE Transactions on Circuits and Systems I: Regular Papers*, 2022.
- [26] M. Ayinala, M. Brown, and K. K. Parhi, "Pipelined parallel FFT architectures via folding transformation," *IEEE Transactions on Very Large Scale Integration Systems*, vol. 20, no. 6, pp. 1068–1081, 2011.
- [27] N. K. Unnikrishnan and K. K. Parhi, "Multi-channel FFT architectures designed via folding and interleaving," in *2022 IEEE International Symposium on Circuits and Systems (ISCAS)*, 2022, pp. 142–146.
- [28] W. Tan, A. Wang, Y. Lao, X. Zhang, and K. K. Parhi, "Pipelined high-throughput NTT architecture for lattice-based cryptography," in *2021 Asian Hardware Oriented Security and Trust Symposium (AsianHOST)*. IEEE, 2021, pp. 1–4.
- [29] W. Tan, B. M. Case, A. Wang, S. Gao, and Y. Lao, "High-speed modular multiplier for lattice-based cryptosystems," *IEEE Transactions on Circuits and Systems II: Express Briefs*, vol. 68, no. 8, pp. 2927–2931, 2021.
- [30] M. Hamburg, "Ed448-goldilocks, a new elliptic curve." *IACR Cryptol. ePrint Arch.*, vol. 2015, p. 625, 2015.
- [31] P. Barrett, "Implementing the rivest shamir and adleman public key encryption algorithm on a standard digital signal processor," in *Conference on the Theory and Application of Cryptographic Techniques*. Springer, 1986, pp. 311–323.
- [32] S. Halevi, Y. Polyakov, and V. Shoup, "An improved RNS variant of the BFV homomorphic encryption scheme," in *Cryptographers' Track at the RSA Conference*. Springer, 2019, pp. 83–105.



Weihang Tan (Graduate Student Member, IEEE) received his B.S., M.S., and Ph.D. degrees in Electrical Engineering from Clemson University, Clemson, SC, USA, in 2018, 2020, and 2022, respectively. His research interests include hardware security and VLSI architecture design for fully homomorphic encryption, post-quantum cryptography, and digital signal processing systems. He is the recipient of the best PhD forum presentation award at the Asian Hardware Oriented Security and Trust Symposium (AsianHOST).



Sin-Wei Chiu (Graduate Student Member, IEEE) received his bachelor's degree in electrical engineering from National Central University, Taiwan, in 2020. He is currently pursuing a Ph.D. degree in electrical engineering at the University of Minnesota, Twin Cities. His current research interests include VLSI architecture design, post-quantum cryptography, and digital signal processing systems.



Antian Wang (Graduate Student Member, IEEE) received his B.E. (2017) in Communication Engineering from Shanghai Maritime University. He is currently pursuing a Ph.D. degree in Clemson University. His research interests include hardware security and VLSI architecture design, and design automation.



Scale Integration Systems Best Paper Award.

Yingjie Lao (Senior Member, IEEE) is currently an assistant professor in the Department of Electrical and Computer Engineering at Clemson University. He received the B.S. degree from Zhejiang University, China, in 2009, and the Ph.D. degree from the Department of Electrical and Computer Engineering at University of Minnesota, Twin Cities in 2015. He is the recipient of an NSF CAREER Award, a Best Paper Award at the International Symposium on Low Power Electronics and Design (ISLPED), and an IEEE Circuits and Systems Society Very Large



Keshab K. Parhi (Fellow, IEEE) is the Erwin A. Kelen Chair in Electrical Engineering and a Distinguished McKnight University Professor in the Department of Electrical and Computer Engineering. He completed his Ph.D. in EECS at the University of California, Berkeley in 1988. He has published over 700 papers, is the inventor of 34 patents, and has authored the textbook *VLSI Digital Signal Processing Systems* (Wiley, 1999). His current research addresses VLSI architectures for machine learning, hardware security, data-driven neuroscience and

DNA computing. Dr. Parhi is the recipient of numerous awards including the 2003 IEEE Kiyoo Tomiyasu Technical Field Award, and the 2017 Mac Van Valkenburg award and the 2012 Charles A. Desoer Technical Achievement award from the IEEE Circuits and Systems Society. He served as the Editor-in-Chief of the *IEEE Trans. Circuits and Systems, Part-I: Regular Papers* during 2004 and 2005. He is a Fellow of the ACM, AIMBE, AAAS, and NAI.